Atmos. Chem. Phys. Discuss., 12, 20717–20743, 2012
www.atmos-chem-phys-discuss.net/12/20717/2012/
doi:10.5194/acpd-12-20717-2012

Atmospheric Chemistry and Physics Discussions

Sea-spray geoengineering in the HadGEM2-ES Earth-system model: radiative impact and climate response

A. Jones and J. M. Haywood

Met Office Hadley Centre, Exeter, UK

Received: 25 June 2012 – Accepted: 6 August 2012 – Published: 17 August 2012

Correspondence to: A. Jones (andy.jones@metoffice.gov.uk)

Published by Copernicus Publications on behalf of the European Geosciences Union.

Abstract

The radiative impact and climate effects of geoengineering using sea-spray aerosols have been investigated in the HadGEM2-ES Earth system model using a fully prognostic treatment of the sea-spray aerosols and also including their direct raditive effect. Two different emission patterns were considered, one to maximise the direct effect in clear skies, the other to maximise the indirect effects of the sea-spray on low clouds; in both cases the emissions were limited to 10 % of the ocean area. While the direct effect was found to be significant, the indirect effects on clouds were much more effective in reducing global mean temperature. Moreover, the impact on global mean precipitation per unit temperature reduction was found to be greatest when the emission pattern for maximising the direct effect was used, suggesting that targeting the direct effect of sea-spray is not a good strategy. The impact on the distribution of precipitation was found to be similar in character, but less in degree, than that simulated by a previous study using a much simpler treatment of this geoengineering process.

1 Introduction

Geoengineering (also known as climate engineering) has recently received some considerable attention owing to the lack of progress in tackling the continued anthropogenic emissions of greenhouse gases (Robock, 2008; Lenton and Vaughan, 2009). These geoengineering schemes broadly fall into two categories: carbon dioxide removal (CDR) schemes which aim to actively remove and hence reduce atmospheric concentrations of CO_2, and solar solar radiation management (SRM) schemes which aim to counter global warming by reflecting an increased proportion of sunlight back to space. While CDR schemes may be considered relatively benign as the ultimate effect on atmospheric CO_2 levels is similar to enhanced mitigation through reduced CO_2 emissions, the costs involved in such schemes are currently prohibitive compared with standard mitigation approaches. Additionally, because the timescales for CDR

ACPD
12, 20717–20743, 2012

implementation and the atmospheric lifetime of CO_2 are relatively long, CDR cannot be used to induce a rapid cooling to counterbalance or even potentially reverse global warming. SRM schemes can theoretically be used to induce such a rapid cooling, with two plausible approaches being the brightening of low-level marine clouds (e.g., Latham, 1990) and the injection of SO_2 or other particles into the stratosphere (e.g., Crutzen, 2006).

Studies of the impact of cloud brightening as a mechanism for geoengineering include those of Latham (1990, 2002); Latham et al. (2008); Rasch et al. (2009) and Jones et al. (2009, 2011) which have concentrated on the impact of the deliberate injection of sea-spray aerosols acting as cloud condenstation nuclei (CCN) into marine clouds, thereby enhancing their albedo and reducing their precipitation efficiency. However, as shown by Partanen et al. (2012), these aerosols are also likely to have a considerable direct effect on solar radiation, the possible climate impacts of which have not yet been considered.

These studies generally suggest that while global mean temperature can indeed theoretically be manipulated to counter global warming, there are inevitably some areas where significant climate changes (in terms of precipitation) still occur. For example, significant decreases in precipitation over Amazonia have been modelled by Jones et al. (2009) when the South Atlantic stratocumulus cloud sheet was artificially brightened. However, this study has some notable limitations: it did not use a prognostic treatment of sea-salt aerosols generated by the model using injection rates relevant to specifically designed ships (Salter et al., 2008). Instead, regions of marine stratocumulus clouds were artificially brightened by assuming an elevated cloud droplet number concentration (CDNC) of 375 cm^{-3}. The location and extent of these brightened regions were assumed, rather than being evaluated in terms of their potential to exert a maximal radiative forcing if such geoengineering ships were deployed. Additionally, sea-spray aerosol generation, microphysics, transport, wet and dry deposition are not explicitly modelled, and the associated direct radiative effect of the aerosol cannot be computed. We address these deficiencies in this study.

ACPD
12, 20717–20743, 2012

Assuming finite resources for sea-spray geoengineering, the question arises as to where such resources should be deployed. In this study we arbitrarily assume that sufficient resources are available to conduct geoengineering operations over 10 % of the ocean's surface (~ 7.1 % of the planet's area). We consider where sea-spray generation should be deployed if consideration is primarily given to (a) the indirect effects or (b) the direct effects of the geoengineered sea-spray. The approach used by Jones et al. (2009) is inadequate for investigating these questions as it simply prescribed CDNC in specific regions and took no account of the direct effects of sea-spray aerosols. Consequently, a full prognostic treatment of geoengineered sea-spray aerosols has been introduced.

2 Modelling geoengineered sea-spray aerosol

The model used in this study is HadGEM2-ES (Collins et al., 2011), the Earth-system configuration of the new Met Office Hadley Centre climate model HadGEM2 (Martin et al., 2011). HadGEM2-ES includes components to model the atmosphere, tropospheric chemistry, aerosols, the land surface and hydrology, the terrestrial carbon cycle, the ocean, sea-ice and ocean biogeochemistry – see Collins et al. (2011) for details.

This model has been extended to include a prognostic treatment of geoengineered sea-spray aerosol. Two variables for sea-spray aerosol are included, one to represent free particles as a log-normal accumulation mode and another for aerosols dissolved in cloud droplets, following the approach of Bellouin et al. (2011). The accumulation mode has the same size and optical parameters as used for natural film-mode sea-salt aerosol in HadGEM2 (median radius 0.1 µm, geometric standard deviation 1.9, density 2165 kg m^{-3}, single-scatter albedo 1.0). The aerosol is hygroscopic and thus acts as a CCN, and the dissolved sea-spray mode allows for effective treatment of wet deposition removal processes. The emission rate follows equation 1 of Korhonen et al. (2010) which relates the number flux of sea-spray aerosol particles to local 10-m windspeed; this flux is injected into the middle of the lowest model layer (20 m above

ACPD
12, 20717–20743, 2012

the surface). Other processes which affect the sea-spray aerosol (transport, interaction with clouds and radiation, wet and dry deposition) are handled in the same manner as with the other aerosol species in HadGEM2 (see Bellouin et al. (2011) for details).

3 Location of emissions

In order to determine the locations for sea-spray generation we evaluate the optimal 10 % of the sea-surface area for the direct and first indirect (cloud albedo) effect using the following method. One-year simulations of the model were run using two calls to the radiation scheme which allowed the radiative forcing from geoengineered sea-spray to be diagnosed whilst not affecting the evolution of the model's meteorology. Sea-spray was emitted over all parts of the ocean at rates given by the expression of Korhonen et al. (2010), reduced proportionately by any sea-ice present. The horizontal advection of the sea-spray aerosol was disabled in these simulations so that the radiative forcing of the aerosol diagnosed at a given point was due only to the local conditions (wind speed, precipitation, cloud cover, insolation etc.) at that point.

Two simulations were performed, one including only the direct effect of the geoengineered sea-spray aerosol, the other including only its first indirect effect. The radiative impact of the second indirect effect on cloud precipitation efficiency cannot be determined by using a double radiation call as it does not act instantaneously. The two distributions of annual mean forcing thus obtained (which, by design, are all over ocean and are co-located point-by-point with the location of emission) were then used as input to an iterative process whereby the regions with the weakest forcing in each distribution were progressively eliminated until only 10 % of the ocean area remained. These two distributions were then assumed to indicate the optimal areas for sea-spray emission when considering either the direct or indirect effects as being of most interest. Unsurprisingly, clear-sky regions in the tropics between about 15° N/S were optimal for the direct effect (a distribution we denote "D-mask"), and sub-tropical stratiform cloud regions in the Pacific, Atlantic and Indian oceans for the indirect effect (denoted "I-mask").

ACPD
12, 20717–20743, 2012

Jones et al. (2009) found that modifications to the stratocumulus region in the South Atlantic had a deleterious effect on precipitation over South America, so a further distribution was determined (I-mask$_{NSA}$) which did not include the South Atlantic. This pattern essentially just increased the extent of the other regions in I-mask to compensate for the lack of the South Atlantic region. All three emission patterns are shown in Fig. 1. Note that we do not claim that this is necessarily the ideal approach for determining optimal emission locations, it is simply a plausible attempt to define these areas within the model. Different approaches are taken by Rasch et al. (2009), Partanen et al. (2012) and Alterskjær et al. (2012), for example.

4 Forcing and radiative flux perturbation

The absolute values of forcing produced in the idealised simulations described above are meaningless as the advection of the sea-spray aerosols is disabled. To investigate the radiative forcing in a more realistic context, three more one-year simulations using each of the three emission patterns were performed. These simulations included both direct and first indirect effects of the sea-spray aerosol, the double radiation-call method to determine the radiative forcing of the combined direct and indirect effects was again used, and this time the sea-spray aerosol was advected as normal. The resulting annual-mean global forcings are given in Table 1 and range from $-0.74\,\mathrm{Wm}^{-2}$ when using I-mask to $-0.58\,\mathrm{Wm}^{-2}$ with D-mask.

Simulations were also performed to determine the forcing for the four combinations of direct effect only, first indirect effect only, I-mask and D-mask. As the meteorology evolved identically in all these experiments, a direct comparison could be made between the resulting forcings, despite the short (1-yr) length of the simulations. As shown in Table 1, when using I-mask the total forcing is split almost exactly 50-50 between the first indirect and direct effects. In contrast, when using D-mask, the majority (almost 80 %) of the combined forcing derives solely from the direct effect.

ACPD
12, 20717–20743, 2012

Although useful to examine the split between the direct and first indirect effects for I-mask and D-mask emission patterns, radiative forcing does not necessarily give a good estimate of the radiative impact of aerosols as it does not take into account the second indirect effect on clouds or any other fast feedback processes. In order to estimate the radiative impact that would actually be exerted in a coupled-model simulation, a set of experiments was performed using the atmosphere-only version of the model (which uses climatological sea-surface tempertaures and sea-ice extents) to estimate the radiative flux perturbation (RFP; Haywood et al., 2009). This set consisted of four 10-yr simulations: a control (no geoengineered sea-spray) and three experiments injecting sea-spray according to the I-mask, D-mask and I-mask$_{NSA}$ emission patterns. All aerosol effects are included in these runs, which evolve differently as the sea-spray aerosols are allowed to interact with the meteorology. The RFP is defined as the difference in top-of-atmosphere net radiation between each experiment and the control.

As shown in Fig. 2 and Table 1, the RFP for I-mask is about 40 % greater than the corresponding forcing (Table 1), most likely due to the inclusion of the second indirect effect in the RFP. In contrast, when using D-mask the resulting RFP is virtually the same as the radiative forcing, suggesting that no significant further effects are invoked when emitting in the D-mask regions. Another difference when using these emission patterns is the lifetime of the geoengineered sea-spray aerosol. When using I-mask the mean lifetime is 4.8 days, increasing by over 30 % to 6.3 days with D-mask. As the point of I-mask and D-mask is to target optimal areas for the indirect and direct effects, respectively, then it follows that I-mask will pick out cloudier regions with more precipitation and therefore wet deposition of aerosols than D-mask, as borne out by the differences in aerosol lifetime.

The mean RFP of $-1.04\,\mathrm{Wm}^{-2}$ for I-mask may be compared with an RFP of $-0.97\,\mathrm{Wm}^{-2}$ obtained by Jones et al. (2009). This earlier study modified a smaller area of cloud, confined to 3.3 % of the Earth's surface, whereas here sea-spray is emitted over 7.1 % of the Earth's surface and is allowed to spread out from the original emission area. However, Jones et al. (2009) also increased CDNC values more: for clouds

ACPD
12, 20717–20743, 2012

at ∼ 1 km in the emission regions, the mean increase in Jones et al. (2009) was more than 200 % compared with ∼ 32 % here. Partanen et al. (2012), who also use a fully prognostic treatment of sea-spray aerosol and include its direct radiative effect, obtain an RFP of $-0.8\,\mathrm{Wm}^{-2}$ when limiting sea-spray emissions to similar regions and areal extent as Jones et al. (2009).

5 Climate impacts

5.1 Experiment design

A set of HadGEM2-ES simulations were used to investigate the potential climate impacts of geoengineered sea-spray. The control was the RCP4.5 simulation performed for CMIP5, the fifth phase of the Climate Model Intercomparison Project (Taylor et al., 2009). The RCP4.5 simulation starts in 2005 and then follows a scenario of changing greenhouse gas concentrations, aerosol emissions and land-use changes such that the anthropogenic forcing in the year 2100 is approximately $4.5\,\mathrm{Wm}^{-2}$ compared with the preindustrial period (Moss et al., 2010). Based on this control, three simulations which included geoengineered sea-spray emissions were initialised in the year 2020 and integrated forwards for 50 yr. The simulations included all modelled forcing effects of the sea-spray aerosol and differed only in which of the three emission patterns described above were used. Geoengineering was terminated after 50 yr and the simulations continued for a further 20 yr. This experimental design follows that of the Geoengineering Model Intercomparison Project (GeoMIP; Kravitz et al., 2011) and allows a comparison of the results presented here with those from the hypothetical stratospheric aerosol solar radiation management simulations of GeoMIP. We include some results from the GeoMIP G4 experiment, which involves continuously emitting 5 Tg[SO_2] per year into the lower stratosphere from 2020 to 2069.

The results presented below are generally means over the final 30 yr of the geoengineering period (2040–2069 inclusive).

ACPD
12, 20717–20743, 2012

5.2 Surface temperature

The mean changes in near-surface air temperature are shown in Fig. 3 and Table 2. Geoengineering using all three emission patterns generates global-mean cooling, but differing considerably in degree. The I-mask and I-mask$_{NSA}$ emission patterns induce similar global-mean changes of -0.54 ± 0.10 K and -0.49 ± 0.11 K, respectively, with the greatest cooling in the sub-tropics over the ocean (i.e. broadly co-located with the emissions) and in the Arctic. The changes in the Arctic are due to the ice-albedo feedback which locally enhances the response to the general global cooling caused by the sea-spray aerosols. In contrast, the temperature response when using the D-mask emission patterns is considerably less at -0.13 ± 0.10 K. There is a diffuse band of cooling in the tropics where the sea-spray aerosol was emitted, but the greatest regional temperature change is again in the Arctic.

The evolution of global-mean near-surface air temperature for the three sea-spray experiments are shown in Fig. 4 along with that from the unmitigated RCP4.5 simulation used as a control; the results from the GeoMIP G4 simulation are also included for reference. The greater effectiveness of the I-mask and I-mask$_{NSA}$ patterns is obvious, although note that the mean temperature in D-mask does differ from RCP4.5 at the 5 % significance level. The cooling in G4 is noticeably greater, due in part to a somewhat larger RFP (-1.37 ± 0.19 Wm^{-2}).

5.3 Precipitation

The changes in annual-mean precipitation rate when using the three different emission patterns are shown in Fig. 5 and Table 2. All three distributions produce decreases in global mean precipitation, equivalent to a -1.3% reduction for I-mask, -0.4% for D-mask and -1.2% for I-mask$_{NSA}$. The greatest changes are in the tropics and sub-tropics, associated with perturbations to the position of the inter-tropical convergence zone (ITCZ), leading to both increases and decreases in regional precipitation. The I-mask and I-mask$_{NSA}$ simulations, which had the largest reductions in surface temper-

ACPD
12, 20717–20743, 2012

ature, also show the largest changes in precipitation; the D-mask simulation, in which there was only a small cooling, has much smaller changes.

Over land, the I-mask simulation generally shows increases north of the equator in the far north of South America, central Africa and India, with decreases to the south of the equator especially in the west of the Amazon basin and the Nordeste region of Brazil. There are also indications of a preciptation reduction in the southern USA. The D-mask simulation has only small changes in precipitation over land, mainly in South America. In I-mask$_{NSA}$ the changes are generally distributed in a simlar pattern to I-mask over land but to a different degree. The precipitation increases are larger over India but smaller over central Africa, there is a greater reduction in precipitation in the southern USA, and an area of statistically significant reduction in Europe. A rather different pattern is seen in South America, which although still showing precipitation reduction in the western Amazon basin, also has a much larger area of increase in the north and northeast of South America, with decreases on the Atlantic coast south of 30° S. There are no significant precipitation changes in the Nordeste region in this simulation.

5.4 Soil moisture

Changes in soil moisture content, shown in Fig. 6, affect vegetation more directly than changes in precipitation. Nevertheless, the changes in soil moisture are often similar to those in precipitation. For I-mask (Fig.6a) there are notable areas of drying in South America and the southern USA, with increases in soil moisture in central Africa and India. Not all changes in soil moisture closely follow changes in precipitation: the increases in high northern latitudes are related to an increased fraction of frozen (and hence immobile) soil moisture in the cooler geoengineered climate. As with temperature and precipitation, the changes with D-mask are much smaller. The changes in the I-mask$_{NSA}$ simulation are again similar to those in precipitation, with the sizable area of drying in northern and eastern Europe being a notable feature.

ACPD
12, 20717–20743, 2012

5.5 Net primary productivity

The impact of geoengineering on the net primary productivity of vegetation (NPP, figure 7) will be a combination of, at the least, its impact on temperature and soil moisture. (Other factors can also be important, such as any impact on the ratio of diffuse to direct solar radiation at the surface, e.g. Mercado et al. (2009).) Some changes in NPP follow those in soil moisture and precipitation: in the I-mask simulation (Fig. 7a) there are NPP reductions in the southern USA and eastern coastal regions of South America, and significant areas of increase, such as central Africa and northern India. Other regions, such as the western Amazon basin, show a drying of soil moisture, but the geoengineered cooling of this heat-stressed region more than compensates for this, giving an increases in NPP. The opposite effect tends to occur at high northern latitudes, where the geoengineered cooling reduces NPP. For I-mask$_{NSA}$, features that were clear in the soil moisture changes are also present in NPP, such as the larger reduction in the southern USA and Europe, and the increase in parts of northern South America. NPP changes in the D-mask simulation are again much smaller.

6 Discussion and conclusions

The simulations used to calculate radiative forcing and RFP indicated that the direct effect of geoengineered sea-spray is not insignificant when compared with its impact on clouds, in agreement with Partanen et al. (2012). Consequently, it was thought useful to assess the impact of sea-spray geoengineering if two emission strategies were followed, one taking the effect on clouds to be most important, the other considering the effect in clear skies as primary. Because such aerosols in the real world will always have both effects depending on their environment, we did not force the sea-spray aerosols in the coupled-model simulations to have only direct or indirect effects. Instead we allowed all aerosol effects to operate and modelled the two different emission strategies by targeting emissions in different areas of the ocean.

ACPD
12, 20717–20743, 2012

The efficiency per unit RFP of the different emission patterns in changing global-mean temperature and precipitation are given in Table 2. The efficiency of cooling when using the D-mask emission pattern for sea-spray geoengineering is less than half that obtained when using the other emission patterns, despite having a burden of geoengineered aerosol about a third higher, consistent with its increased lifetime. This appears to be related to a feedback via clouds. In the simulations with fixed sea-surface temperatures used to determine the RFP, emitting sea-spray aerosols using the D-mask emission pattern caused little change in net cloud forcing ($+0.04\,\mathrm{Wm}^{-2}$ in the global mean, only $2.5\times10^{-4}\,\mathrm{Wm}^{-2}$ for the region between 30° N/S). However, in the fully-coupled simulations with D-mask, net cloud forcing is changed much more, especially in the tropics ($+0.16\,\mathrm{Wm}^{-2}$ in the global mean, $+0.32\,\mathrm{Wm}^{-2}$ bewteen 30° N/S). This reduction in the cooling impact of cloud will contribute to the reduced impact of geoengineering on surface temperature in this case. When comparing changes in global mean precipitation, although the reduction in D-mask is much smaller in absolute terms than I-mask or I-mask$_{\mathrm{NSA}}$ (Table 2), per unit global cooling it in fact produces ∼ 50 % greater reduction in precipitation. These results suggest that, although it is important to consider the direct radiative effect of geoengineered sea-spray aerosols, it would be inefficient to concentrate on this aspect of their effect and that their impact on clouds is indeed of primary importance for this form of geoengineering.

One of the main results from a previous study (Jones et al., 2009) was the negative impact on precipitation over parts of South America by geoengineering stratocumulus clouds in the South Atlantic. This was the reason for defining the I-mask$_{\mathrm{NSA}}$ emission pattern, to exclude from modification the South Atlantic region present in I-mask. Figure 8 shows a comparison of the the percentage change in 30-yr mean precipitation over the central and southern Pacific/Atlantic regions from the results of Jones et al. (2009) (Fig.8a) compared with those from I-mask and I-mask$_{\mathrm{NSA}}$ (Figs. 8b and 8c, respectively). The patterns of change are broadly similar, differing mainly in the magnitude of the changes, not their distribution. There is obviously less impact over the north of South America in I-mask compared with the results of Jones et al. (2009),

ACPD
12, 20717–20743, 2012

which might be expected given the different manner the geoengineering was simulated in each case. The global mean RFP in both cases is very similar, but in Jones et al. (2009) the local RFP is large and concentrated in small regions (see Fig. 9), whereas in the present study it is more diffuse, with smaller values over a larger area (Fig. 2a). Consequently, the RFP in I-mask is not as inhomogeneous as in Jones et al. (2009) and so the regional impact is reduced (Jones et al., 2011).

If geoengineered sea-spray emissions in the South Atlantic are avoided (Fig.8c) there are smaller areas of reduction in precipitation over the north of South America and larger areas of increase, but in many ways the pattern is not fundamentally altered. The northward movement of the precipitation maximum associated with the ITCZ in the Atlantic is still evident, and although the degree to which this shift affects precipitation over land does not appear too large in this simulation, it would only take a small change in the position of the ITCZ to have a much greater impact, as can be seen from the large areas of change just offshore. Any process which affects the position of the ITCZ and the large amount of precipitation associated with it will have an impact on adjacent ecosystems and their populations. These impacts could be positive as well as negative: for example, while precipitation and NPP decrease in the Nordeste region, they increase in sub-Saharan Africa in all three simulations considered in Fig. 8. Additionally, while we have concentrated on precipitation changes over large land-masses, the impact of any changes in seasonal rainfall patterns on small island communities should not be forgotten.

It is also interesting to compare the mean results from the three experiments using sea-spray geoengineering with those from the GeoMIP G4 experiment which injects SO_2 into the lower stratosphere (Table 2). The RFP in G4 is greater than produced by sea-spray geoengineering, but of a similar order of magnitude. G4 shows the greatest efficiency in reducing global-mean temperature per unit RFP and has the lowest impact on global-mean precipitation per unit cooling.

The main conclusions from this study are (1) that the direct radiative effect of geoengineered sea-spray aerosol in clear skies is significant and should be taken into

ACPD
12, 20717–20743, 2012

account, but that its indirect effect on clouds is of greater importance; (2) that targeting sea-spray emissions to maximise indirect effects is a better strategy for reducing global mean temperature while minimising precipitation changes than using emission patterns which maximise the direct effect; and (3) that the more detailed treatment of sea-spray aerosols shows impacts on climate (specifically precipitation) which are similar in character, though reduced in degree, to those obtained previously using a much simpler treatment. Such conclusions may of course be model dependent, which emphasises the importance of initiatives such as GeoMIP in attempting a more general consensus.

Acknowledgements. This work was supported by the Joint DECC/Defra Met Office Hadley Centre Climate Programme (GA01101) and by a joint EPSRC/NERC initiative via the Integrated Assessment of Geoengineering Proposals (IAGP; http://www.iagp.ac.uk/), contract number EPSRC EP/I014721/1.

References

Alterskjær, K., Kristjánsson, J. E., and Seland, Ø.: Sensitivity to deliberate sea salt seeding of marine clouds – observations and model simulations, Atmos. Chem. Phys., 12, 2795–2807, doi:10.5194/acp-12-2795-2012, 2012. 20722

Bellouin, N., Rae, J., Jones, A., Johnson, C., Haywood, J., and Boucher, O.: Aerosol forcing in the Climate Model Intercomparison Project (CMIP5) simulations by HadGEM2-ES and the role of ammonium nitrate, J. Geophys. Res., 116, D20206, doi:10.1029/2011JD016074, 2011. 20720, 20721

Collins, W. J., Bellouin, N., Doutriaux-Boucher, M., Gedney, N., Halloran, P. Hinton, T., Hughes, J., Jones, C. D., Joshi, M., Liddicoat, S., Martin, G., O'Connor, F., Rae, J., Senior, C., Sitch, S., Totterdell, I., Wiltshire, A., and Woodward, S.: Development and evaluation of an Earth-system model - HadGEM2, Geosci. Model Dev., 4, 1051–1075, doi:10.5194/gmd-4-1051-2011, 2011. 20720

ACPD
12, 20717–20743, 2012

Crutzen, P.: Albedo enhancement by stratospheric sulfur injections: A contribution to resolve a policy dilemma?, Clim. Change, 77, 211–220, doi:10.1007/s10584-006-9101-y, 2006. 20719

Haywood, J., Donner, L., Jones, A., and Golaz, J.-C.: Global indirect radiative forcing caused by aerosols: IPCC (2007) and beyond, in: Clouds in the Perturbed Climate System: Their Relationship to Energy Balance, Atmospheric Dynamics, and Precipitation, Strüngmann Forum Report, edited by: Heintzenberg, J. and Charlson, R. J., MIT Press, Cambridge, USA, 451–467, 2009. 20723

Jones, A., Haywood, J., and Boucher, O.: Climate impacts of geoengineering marine stratocumulus clouds, J. Geophys. Res., 114, D10106, doi:10.1029/2008JD011450, 2009. 20719, 20720, 20722, 20723, 20724, 20728, 20729, 20742, 20743

Jones, A., Haywood, J., and Boucher, O.: A comparison of the climate impacts of geoengineering by stratospheric SO_2 injection and by brightening of marine stratocumulus cloud, Atmos. Sci. Lett., 12, 176–183, doi:10.1002/asl.291, 2011. 20719, 20729

Korhonen, H., Carslaw, K. S., and Romakkaniemi, R.: Enhancement of marine cloud albedo via controlled sea spray injections: a global model study of the influence of emission rates, microphysics and transport, Atmos. Chem. Phys., 10, 4133–4143, doi:10.5194/acp-10-4133-2010, 2010. 20720, 20721

Kravitz, B., Robock, A., Boucher, O., Schmidt, H., Taylor, K., Stenchikov, G., and Schulz, M.: The Geoengineering Model Intercomparison Project (GeoMIP), Atmos. Sci. Lett., 12, 162–167, doi:10.1002/asl.316, 2011. 20724

Latham, J.: Control of global warming? Nature, 347, 339–340, doi:10.1038/347339b0, 1990. 20719

Latham, J.: Amelioration of global warming by controlled enhancement of the albedo and longevity of low-level maritime clouds, Atmos. Sci. Lett., 3, 52–58, doi:10.1006/Asle.2002.0048, 2002. 20719

Latham, J., Rasch, P., Chen, C.-C., Kettles, L., Gadian, A., Gettelman, A., Morrison, H., Bower, K., and Choularton, T.: Global temperature stabilization via controlled albedo enhancement of low-level maritime clouds, Phil. Trans. R. Soc. A, 366, 3969–3987, doi:10.1098/rsta.2008.0137, 2008. 20719

Lenton, T. M. and Vaughan, N. E.: The radiative forcing potential of different climate geoengineering options, Atmos. Chem. Phys., 9, 5539–5561, doi:10.5194/acp-9-5539-2009, 2009. 20718

ACPD
12, 20717–20743, 2012

Martin, G. M., Bellouin, N., Collins, W. J., Culverwell, I. D., Halloran, P. Hardiman, S., Hinton, T. J., Jones, C. D., McLaren, A., O'Connor, F., Rodriguez, J., Woodward, S., Best, M., Brooks, M. E., Brown, A. R., Butchart, N., Dearden, C., Derbyshire, S. H., Dharssi, I., Doutriaux-Boucher, M., Edwards, J. M., Falloon, P., Gedney, N., Gray, L., Hobson, M., Huddleston, M., Hughes, J., Ineson, S., Ingram, W., James, P. M., Johns, T. C., Johnson, C., Jones, A., Jones, C. P., Joshi, M., Liddicoat, S., Lock, A. P., Maidens, A., Milton, S. F. , Rae, J., Sellar, A., Senior, C. A., Totterdell, I., Verhoef, A., Vidale, P. L., and Wiltshire, A.: The HadGEM2 family of Met Office Unified Model climate configurations, Geosci. Model Dev., 4, 723–757, doi:10.5194/gmd-4-723-2011, 2011. 20720

Mercado, L., Bellouin, N., Boucher, O., Sitch, S., Huntingford, C., Wild, M., and Cox, P.: Impact of changes in diffuse radiation on the global land carbon sink, Nature, 458, 1014–1017, doi:10.1038/nature07949, 2009. 20727

Moss, R. H., Edmonds, J. A., Hibbard, K. A., Manning, M. R., Rose, S. K., van Vuuren, D. P., Carter, T. R., Emori, S., Kainuma, M., Kram, T., Meehl, G. A., Mitchell, J. F. B., Nakicenovic, N., Riahi, K., Smith, S. J., Stouffer, R. J., Thomson, A. M., Weyant, J. P., and Wilbanks, T. J.: The next generation of scenarios for climate change research and assessment, Nature, 463, 747–756, doi:10.1038/nature08823, 2010. 20724

Partanen, A.-I., Kokkola, H., Romakkaniemi, R., Kerminen, V.-M., Lehtinen, K. E. J., Bergman, T., Arola, A., and Korhonen, H.: Direct and indirect effects of sea spray geoengineering and the role of injected particle size, J. Geophys. Res., 117, D02203, doi:10.1029/2011JD016428, 2012. 20719, 20722, 20724, 20727

Rasch, P. J., Latham, J., and Chen, C.-C.: Geoengineering by cloud seeding: influence on sea ice and climate system, Environ. Res. Lett., 4, 045112, doi:10.1088/1748-9326/4/4/045112, 2009. 20719, 20722

Robock, A.: 20 reasons why geoengineering may be a bad idea, Bull. Atomic Scientists, 64, 14–18, doi:10.2968/064002006, 2008. 20718

Salter, S., Sortino, G., and Latham, J.: Sea-going hardware for the cloud albedo method of reversing global warming, Phil. Trans. R. Soc. A, 366, 3989–4006, doi:10.1098/rsta.2008.0136, 2008. 20719

Taylor, K. E., Stouffer, R. J., and Meehl, G. A.: A summary of the CMIP5 experimental design, Report of the World Climate Research Program, Geneva, Switzerland, available at: http://cmip-pcmdi.llnl.gov/cmip5/experiment_design.html, 2009. 20724

ACPD
12, 20717–20743, 2012

Table 1. Forcing (ΔF) and radiative flux perturbation (RFP) for geoengineered sea-spray using the three different emission patterns (Wm^{-2}). The forcings are from 1-yr runs using two calls to the model's radiation scheme, while the RFP values are given as 10-yr means ± one standard deviation. Separate forcing simulations for direct and indirect effects were not performed for the I-mask$_{NSA}$ case.

	D-mask	I-mask	I-mask$_{NSA}$
ΔF_{direct}	−0.45	−0.37	–
$\Delta F_{1st\ indirect}$	−0.13	−0.38	–
ΔF_{total}	−0.58	−0.74	−0.72
RFP	−0.58 ± 0.10	−1.04 ± 0.08	−0.81 ± 0.10

ACPD
12, 20717–20743, 2012

Table 2. RFPs (Wm^{-2}), global-mean changes in near-surface temperature (K) and precipitation rate ($mm\,day^{-1}$), the efficiency per unit RFP of the change in temperature (K/Wm^{-2}) and the change in precipitation per unit change in temperature ($mm\,day^{-1}/K$).

	RFP	ΔT	Δppn	$\frac{\Delta T}{RFP}$	$\frac{\Delta ppn}{\Delta T}$
D-mask	−0.58	−0.13	−0.014	0.22	0.113
I-mask	−1.04	−0.54	−0.042	0.52	0.077
$I\text{-mask}_{NSA}$	−0.81	−0.49	−0.037	0.61	0.075
G4	−1.37	−0.97	−0.067	0.71	0.069

ACPD
12, 20717–20743, 2012

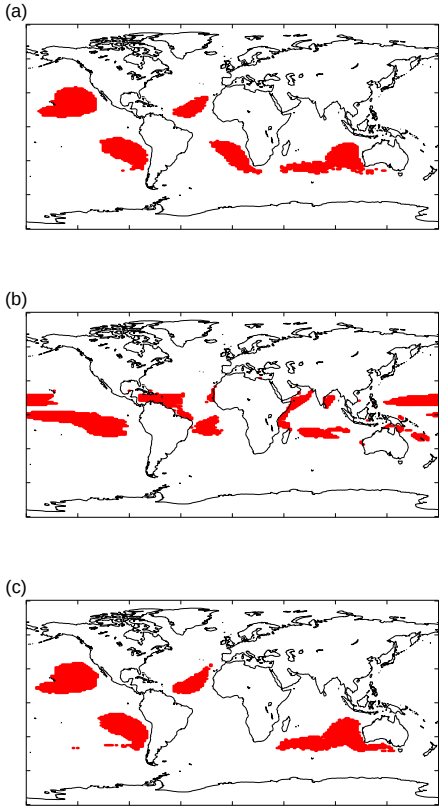

Fig. 1. The three different emission patterns used in this study: **(a)** I-mask; **(b)** D-mask; **(c)** I-mask$_{NSA}$.

ACPD
12, 20717–20743, 2012

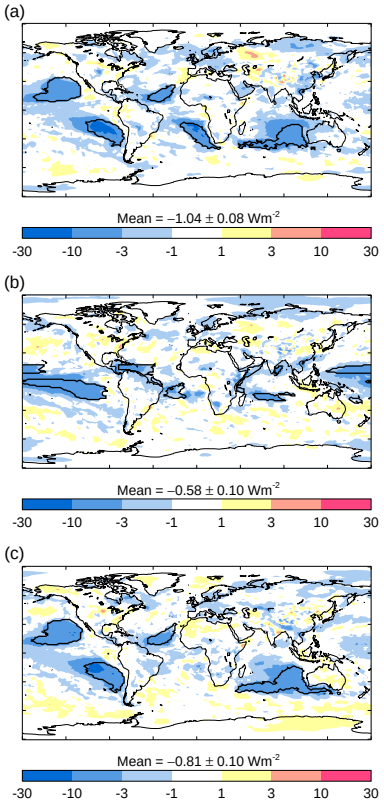

Fig. 2. RFPs due to geoengineered sea-spray aerosols using the different emission patterns, which are indicated by the thick black lines. The 10-yr mean value ± one standard devation is also given. **(a)** I-mask; **(b)** D-mask; **(c)** I-mask$_{NSA}$.

ACPD
12, 20717–20743, 2012

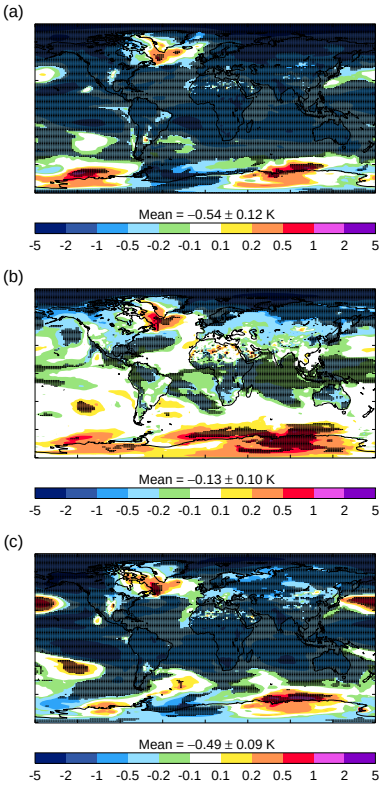

Fig. 3. (a) Mean 2040–2069 change in near-surface air temperature (K) when using the I-mask pattern for emitting geoengineered sea-spray. **(b)** As **(a)** but using the D-mask emission pattern. **(c)** As **(a)** but using I-mask$_{NSA}$. Areas where the changes are significant at the 5 % level are shaded.

ACPD
12, 20717–20743, 2012

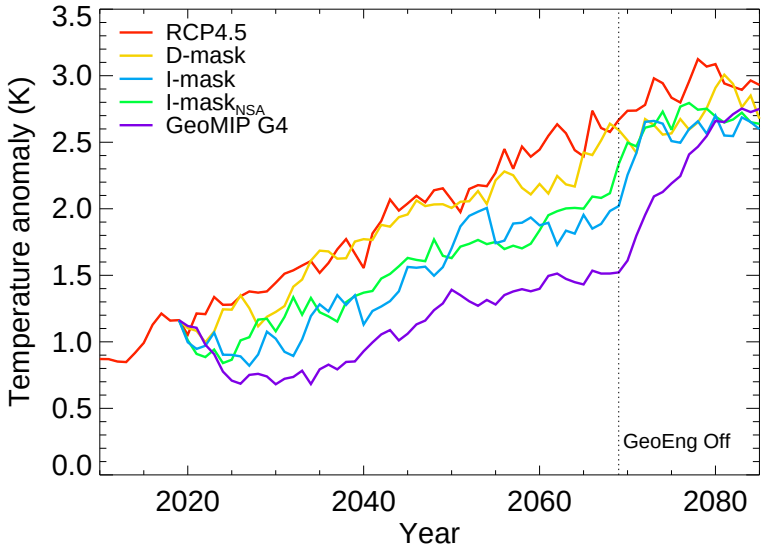

Fig. 4. Evolution of global-mean near-surface temperature anomaly (K) with respect to the pre-industrial mean.

ACPD
12, 20717–20743, 2012

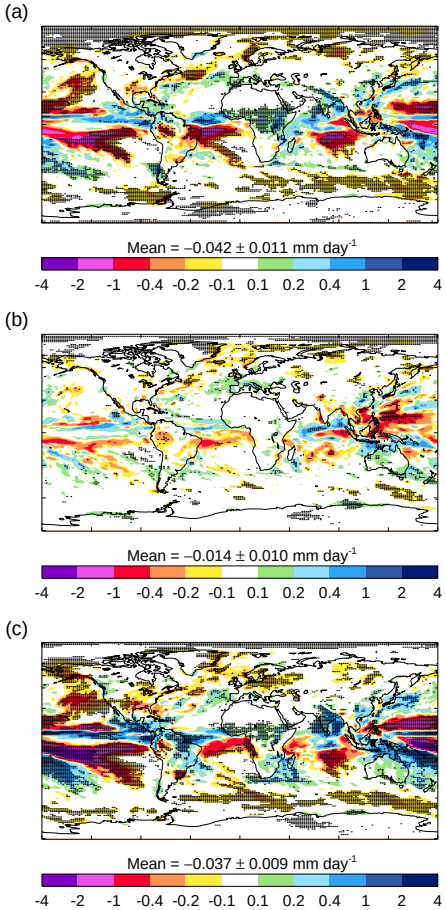

Fig. 5. As figure 3 but for mean 2040–2069 changes in precipitation rate (mm day^{-1}).

ACPD
12, 20717–20743, 2012

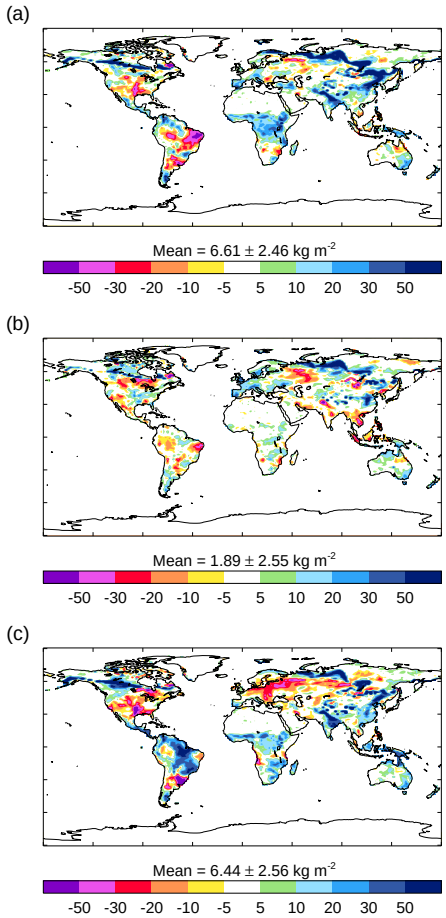

Fig. 6. (a) Mean 2040–2069 change in soil moisture content ($kg\,m^{-2}$) when using the I-mask distribution for emitting geoengineered sea-spray. **(b)** As **(a)** but using the D-mask emission pattern. **(c)** As (a) but using I-mask$_{NSA}$.

ACPD
12, 20717–20743, 2012

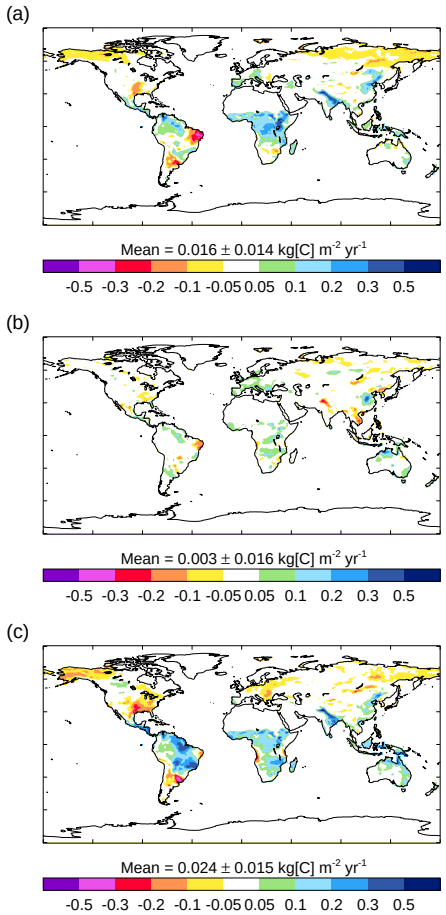

Fig. 7. As Fig. 6 but for mean 2040–2069 changes in vegetation net primary productivity (kg[C] $m^{-2}\,yr^{-1}$).

ACPD
12, 20717–20743, 2012

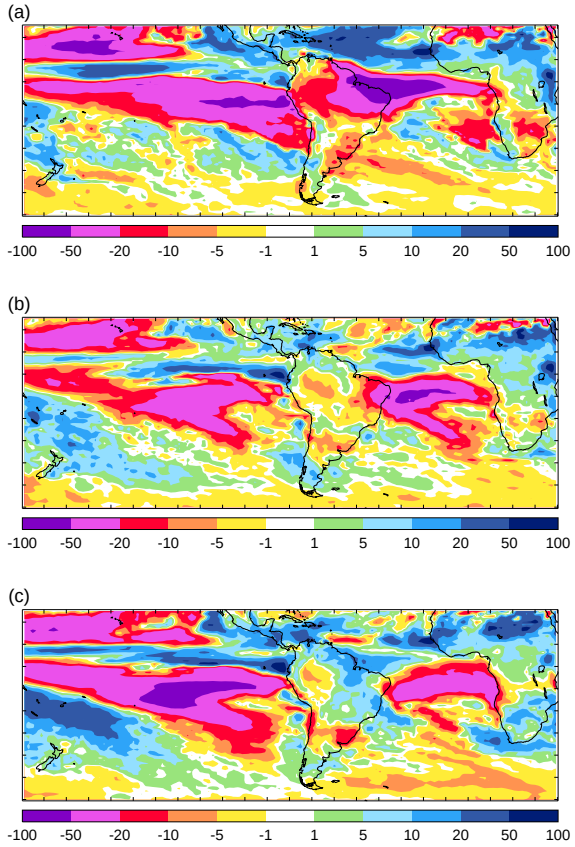

Fig. 8. **(a)** Percentage change in precipitation from the "ALL" case of Jones et al. (2009). **(b)** As **(a)** but for IND-mask. **(c)** As **(a)** but for IND-mask$_{NSA}$.

ACPD
12, 20717–20743, 2012

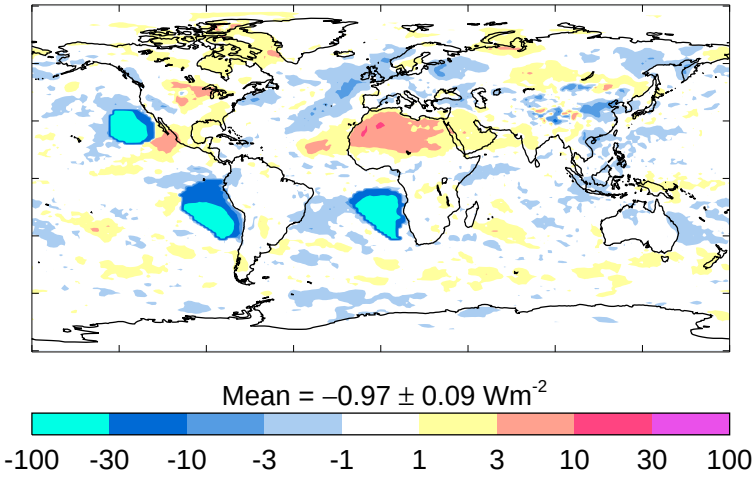

Fig. 9. RFP (Wm^{-2}) due to modified marine stratocumulus clouds from Jones et al. (2009) (Wm^{-2}).

ACPD
12, 20717–20743, 2012